International Journal of Applied Engineering Research ISSN 0973-4562 Volume 13, Number 1 (2018) pp. 245-251

Development of Iron Doped Manganese oxide ($Mn_{2-x}Fe_xO_3$) Catalysts for Soot Oxidation Applications

Satya Deepika Neelapala [1], Abhishek Shetty [2], Gaurav Gaggar [3], Rajat Mall [4] and Harshini Dasari [5,*]

[1]Project Assistant, Department of Chemical Engineering, Manipal Institute of Technology, Manipal Academy of Higher Education, Manipal, Karnataka, India.

[2,3,4] B.Tech Student, Department of Chemical Engineering, Manipal Institute of Technology, Manipal Academy of Higher Education, Manipal, Karnataka, India.

[5]Associate Professor, Department of Chemical Engineering, Manipal Institute of Technology, Manipal Academy of Higher Education, Manipal, Karnataka, India.

[1]Orcid Id: 0000-0003-4206-1971, [2]Orcid Id: 0000-0002-2766-438X, [3]Orcid Id: 0000-0002-1308-8692

[4]Orcid Id: 0000-0002-3844-0066, [5]Orcid Id: 0000-0001-9410-4369

Abstract

This work deals with the catalytic soot oxidation using pure Manganese (III) oxide and Iron doped Mn_2O_3 catalysts. The compounds Mn_2O_3 and the Iron (Fe) doped oxide series $Mn_{2-x}Fe_xO_3$ were synthesized using the method of coprecipitation. All the materials fabricated were characterized using XRD, BET, XPS and SEM analysis. XRD analysis has clearly confirmed the formation of solid solution in all the Fe doped catalysts (till x=0.2). Presence of multiple oxidation states in both Mn and Fe was noted in the prepared samples using XPS analysis. This redox ability of both Mn and Fe has increased the number of oxygen vacancies in $Mn_{2-x}Fe_xO_3$ samples. The Higher amount of adsorbed oxygen is noted in the sample with x=0.2. SEM analysis showed that increase in Fe doping has increased the porosity of the samples. The activity of oxidation of soot by the catalysts was evaluated with instrumental TGA analysis where soot and the synthesized catalyst were in tight contact. Amongst the synthesized catalysts $Mn_{1.8}Fe_{0.2}O_3$ exhibited better catalytic performance due to good porous structure and surface area along with the presence of higher oxygen vacancies.

Keywords: $Mn_{2-x}Fe_xO_3$, Soot Oxidation, Redox ability, surface adsorbed oxygen

INTRODUCTION

Soot is a mixture of impure multi-component particles of carbon resulted from the partial combustion of carbon fuels, coal etc.[1]. Emanation of soot from diesel engines or any other source of vehicles for that matter causes environmental pollution and also carcinogenic to living beings [2]. Continuous exposure to soot is dangerous also leads to cardiovascular and lung diseases. Though diesel engines are considered to be the most effective drive units due to their higher fuel economy and lesser CO_2 emission, they contribute to a major source of soot emission [3]. So, control or removal of soot emission is quintessential for a better environment and also to make the most economical diesel engine feasible to operate under pollution control constraints. Since many years Diesel Particulate Filters (DPF) were widely used in vehicles which operate by trapping the soot particles on the filter with the exhaust gases flowing through them [4,5]. Thus, accumulated soot increases in thickness with respect to time leading to back pressure resulting in decreased engine efficiency. Hence the regeneration of the DPF is always essential and continuously regenerating trap (CRT) techniques were widely employed in Heavy-duty diesel engines [6]. During, the CRT process continuous oxidation of deposited soot by O_2 takes place. Another practice that is in the wide application is the use of FBC's (Fuel Borne Catalysts) that minimizes the soot output and results in enhancement of soot oxidation reaction in DPF [7]. Nonetheless, these catalysts are expensive or mostly radioactive or easily deactivated by sulfur species [8].

On the other hand by using catalytic DPF which supports Catalyst/Soot oxidation reaction at low temperature has become a promising option. Therefore, present researchers are working on developing catalysts which are economically viable, effective in soot oxidation and also can reduce the ignition temperature of soot [9]. In this context, it is worth mentioning that both iron oxide and manganese oxide catalysts are highly active, inexpensive, easily available, earth-abundant and eco-friendly for many oxidation reactions [10,11]. Iron oxide is exclusively active for soot oxidation reaction. Manganese oxide combined with other metal oxides exhibits excellent performance in soot oxidation which is mainly because, both the elements can exist in multiple oxidation states(redox stability) (Mn exists in +2, +3 and +4 while Fe exists in both +2 and +3 oxidation states) [12,13]. Hence, this drives in a motivation to work on Fe-doped Manganese oxide catalysts $Mn_{2-x}Fe_xO_3$ (x=0.05 to 0.2) for the application of soot oxidation reactions. In this work, partial incorporation of Fe into the Mn_2O_3 lattice had led to an improved redox property of the metal cations and subsequent formation of highly reactive adsorbed oxygen species and has shown an improvement in soot oxidation activity.

EXPERIMENTAL METHODS

Catalyst Preparation

Mn_2O_3 and Fe-doped Mn_2O_3 catalysts $Mn_{2-x}Fe_xO_3$ (x= 0.05 to 0.2) were synthesized by Co-Precipitation of metal nitrates salts with Ammonium Hydroxide solution [14]. Iron (III) Nitrate nonahydrate ($Fe(NO_3)_3.9H_2O$_404g/mole) and Manganese (II) Nitrate Tetrahydrate ($Mn(NO_3)_2.4H_2O$_251.01g/mole) salts were taken in aqueous form in proper amounts and precipitated using Ammonium Hydroxide (NH_4OH). In a typical synthesis

of $Mn_{1.95}Fe_{0.05}O_3$, 17.67g of $Mn(NO_3)_2.4H_2O$ and 0.7294g of $Fe(NO_3)_3.9H_2O$ was dissolved in 100ml of distilled water and stirred using a magnetic stirrer. This metal solution was then precipitated by the dropwise addition of NH_4OH solution until pH reached 10. The resultant precipitate was dried at 90˚C for 6h and calcined at 600 ˚C for 6h to obtain the final product. The concentration of NH_4OH used was kept constant for all the other dopant levels.

Characterization

The Phase-Structural analysis of the materials was done by Rigaku Miniflux 6000, X-ray diffractometer with monochromatized high-intensity Cu Ka radiation (λ=1.54 A˚) at a scanning rate of 1˚/min in the 2Θ scanning range of 10˚ - 80˚. FESEM micrographs were obtained by Hitachi S-1460 using AC voltage of 15 kV. Specific Surface Area was determined by BET surface area analyzer (Model-SmartSorb 92/93) where all the samples were evacuated at 200˚C to remove the residual moisture. The XPS analysis of the materials was accomplished using a Thermo K-5 Alpha XPS instrument with the X-ray source Mg Kα (1253.6 eV) radiation.

Catalytic Soot Oxidation Activity

The oxidation of soot in the presence of thus synthesized catalysts was evaluated using Thermogravimetric Analyser (TG-DTA) instrument. The measurements were performed with soot-catalyst mixtures (ground in an agate mortar) in 1:4 weight ratios wherein PRINTEX-U was the model soot used under 'tight contact' condition. The catalytic performance in the oxidation of soot was quantified in terms of $T_{1/2}$ ˚C, the temperature at 50% soot conversion.

RESULTS

XRD Analysis

Figure.1 depicts the Diffraction patterns of $Mn_{2-x}Fe_xO_3$ (x=0 to 0.2) catalysts. All the samples exhibited patterns similar to pure Mn_2O_3 [15] which is of cubic structure. The diffraction patterns of the Fe-doped Mn_2O_3 samples $Mn_{2-x}Fe_xO_3$ (x=0.05 to 0.2) revealed the presence of cubic structure in Mn_2O_3. Hence, from the results obtained it confirms that the cubic structure of Mn_2O_3 was not disturbed till the Fe dopant level reached 0.2 ($Mn_{1.8}Fe_{0.2}O_3$). No peaks of iron oxide were seen in any of the XRD patterns indicating the formation of solid solution in all the samples. The most intense diffraction peak of Mn_2O_3 at around 2Theta~32.5˚ was maintained in all the catalysts synthesized. The specific surface area and pore volumes of the undoped Mn_2O_3 and Fe-doped $Mn_{2-x}Fe_xO_3$ (x=0.05 to 0.2) were tabulated in Table 1. The results depicted that among all the samples $Mn_{1.8}Fe_{0.2}O_3$ showed the higher surface area of 12 m^2/g and a higher pore volume comparatively.

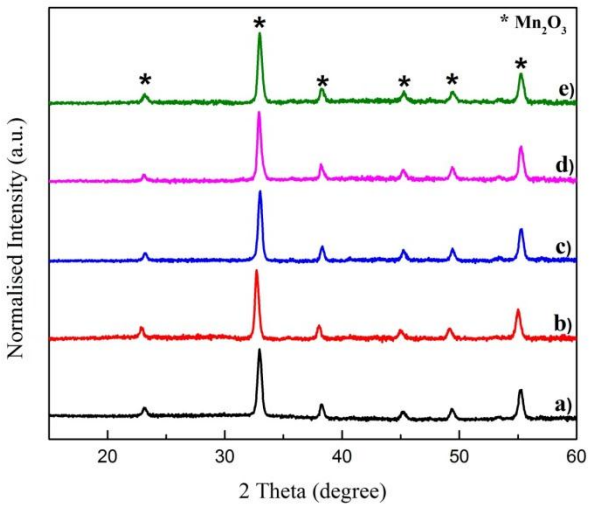

Figure 1: XRD Pattern of all the prepared samples a) Mn_2O_3, b) $Mn_{1.95}Fe_{0.05}O_3$, c) $Mn_{1.9}Fe_{0.1}O_3$, d) $Mn_{1.85}Fe_{0.15}O_3$, and e) $Mn_{1.8}Fe_{0.2}O_3$

Table 1: Crystal size, Lattice parameter, and BET specific surface of the synthesized catalysts.

S. No	Sample	2Theta (degree)	Crystal size (nm)	Lattice Parameter (A^o)	Surface Area (m^2/g)
1.	Mn_2O_3	32.94	20.39	5.057	9.82
2.	$Mn_{1.95}Fe_{0.05}O_3$	32.84	25.02	5.071	4.88
3.	$Mn_{1.9}Fe_{0.1}O_3$	32.93	23.79	5.057	8.63
4.	$Mn_{1.85}Fe_{0.15}O_3$	32.88	22.1	5.103	6.59
5.	$Mn_{1.8}Fe_{0.2}O_3$	32.72	21.14	5.064	10.53

The Lattice parameters and average crystal sizes of all samples were calculated by Debye-Scherer equation by utilizing FWHM (Full Width Half Maximum) [16]. According to the literature, both Fe and Mn has multiple oxidation states with the ionic radii given as, Fe^{+2} with 0.078nm and Fe^{+3} with 0.0645nm, Mn^{+2} with 0.058nm, Mn^{+3} with 0.066nm and Mn^{+4} with 0.053nm [17,18]. The crystal size and the lattice parameters of all the Fe doped samples are higher than that of Mn_2O_3 sample. This suggests the there is a lattice expansion in the materials due to the doping of Fe, into Mn lattice (increase in lattice parameter). Fe^{+2} ions might be dominant in these samples (the ionic radii of all Mn ions are smaller than Fe^{+2}), as the incorporation of material with higher ionic radius will expand the lattice, thereby increasing the crystallite size [19]. No particular trend in lattice parameter was noticed in Fe doped samples with the increase in Fe loading. This might be due to the presence of multiple oxidation states in both Fe and Mn, which has led to either of lattice expansion/ contraction in the samples. It is difficult at this moment to decide the existence of multi oxidation states of Mn and Fe in the prepared materials only from the XRD results. Therefore further investigation on

confirmation of oxidation states using XPS analysis was performed.

XPS Analysis

The presence of iron in the catalysts was not observed in the XRD analysis, so in order to reveal the presence of Fe ions and also to confirm the presence of multiple oxidation states in Fe and Mn, the X-ray Photon Spectra of the catalysts was performed and the results are detailed in the Figure.2, representing the core level spectra of Mn2p, Fe 2p, and O1s. Soot oxidation reaction occurs at the surface/interface between the soot and catalyst and so it is essential to understand the oxidation states of the species involved (Mn, Fe, and O) in the materials [20].

The oxidation states of Mn were determined using the XPS of Mn 2p core level spectra as shown in the Figure.2(a). From the figure, it is evident that the $Mn2p_{3/2}$ peak was around 641.3 eV and Mn $2p_{1/2}$ peak was around 652.9 eV with a spin energy gap of 11.6 eV signifying the presence of Mn^{+3} oxidation state in the material [21]. The literature states that the peak at around 640eV in the $Mn2p_{3/2}$ region is attributed to Mn^{2+} cations while the peaks at 642 eV represent Mn^{4+} oxidation state [22]. However, due to the overlapping of the peaks at around 640-643 eV, the oxidation states cannot be clearly noted from the Figure.2(a). So, for the clear understanding of the Mn phases in this region, deconvolution of the peaks was performed for all the samples (shown in Figure.2(b)) and the % Mn species present in the samples are represented in Table 2. From the figure and table, it can be clearly seen that Mn has multiple oxidation states in all the samples. It can be noted from the table that in Mn_2O_3 sample, Mn has multiple oxidation states like +3 and +4, while in all other Fe doped samples Mn is in +2, +3 and +4 oxidation states. This redox ability in Mn might increase the oxygen vacancies in the samples thereby influencing the soot oxidation activity [23].

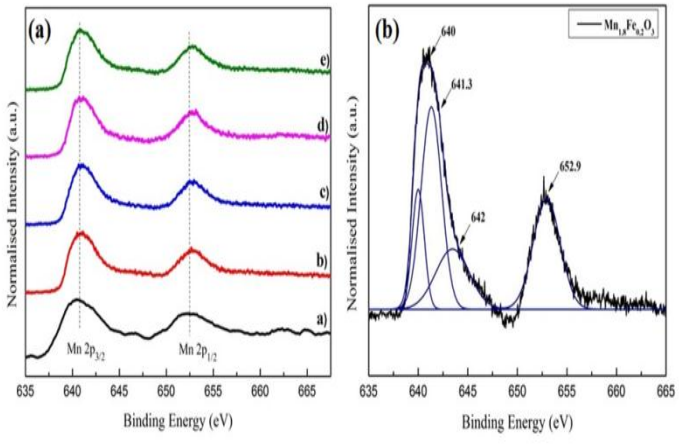

Figure 2: (a) XPS of Mn 2p core level spectra for all the prepared samples, where a) Mn_2O_3, b) $Mn_{1.95}Fe_{0.05}O_3$, c) $Mn_{1.9}Fe_{0.1}O_3$, d) $Mn_{1.85}Fe_{0.15}O_3$, e) $Mn_{1.8}Fe_{0.2}O_3$ and **(b)** Image of Deconvoluted peaks for $Mn_{1.8}Fe_{0.2}O_3$ sample

Figure.3(a) shows the XP spectrum of Fe2p core level region in all the Fe doped samples, wherein the binding energies of Fe $2p_{3/2}$ and Fe $2p_{1/2}$ were at 710 and 723.9 eV respectively corresponding to the presence of Fe^{3+} cations [24]. The satellite peak for Fe $2p_{3/2}$ was observed at 716.9 eV and the difference between the binding energies is approximately 6eV clearly evidences the presence of Fe^{2+} cations [25]. Also, the Fe $2p_{3/2}$ peak can be deconvoluted to two peaks (Figure.3(b)) one at 710 eV corresponding to Fe^{3+} ions and other at around 712.4 eV attributed to the presence of Fe^{+2} cations [26]. All these results confirm the existence of multiple oxidation states of Iron (Fe^{3+}/Fe^{2+}). The percentage of Fe species after the deconvolution is shown in **Table 2**. It can be seen from the table that Fe^{+2} cations are dominant in all the samples which have led to the lattice expansion as confirmed by XRD analysis. The presence of iron in two different oxidation states might increase the surface adsorbed oxygen noticeably, thereby influencing the soot oxidation process [27,28].

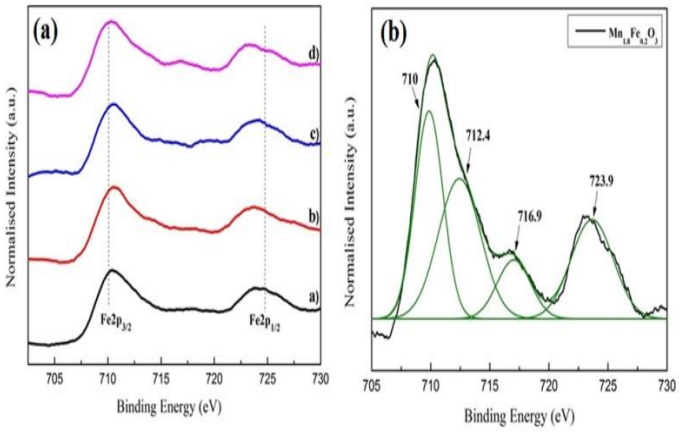

Figure 3: (a) XPS of Fe 2p core level spectra for all Fe doped Mn_2O_3 samples, Where a) $Mn_{1.95}Fe_{0.05}O_3$, b) $Mn_{1.9}Fe_{0.1}O_3$, c) $Mn_{1.85}Fe_{0.15}O_3$, d) $Mn_{1.8}Fe_{0.2}O_3$ and **(b)** Image of Deconvoluted peaks for $Mn_{1.8}Fe_{0.2}O_3$ sample

XPS of O 1s region revealed the existence of two different kinds of oxygen species namely lattice oxygen species (O_{lat}) at a lower binding energy 528 eV approximately shown in Figure.4 and at a higher binding energy around 531.1eV related to adsorbed oxygen species (O_{ads}) [29]. Table 2 provides the data on the % of O_{ads} and O_{lat} in all the samples. It can be seen from the table that % of O_{ads} increased with Fe doping when compared to Mn_2O_3 sample. It can be clearly understood from this that doping of iron into Mn_2O_3 lattice has increased the oxygen vacancies [30]. Presence of redox ability in both Fe and Mn, as evidenced by the XPS analysis for Mn2p and Fe 2p spectra and also the lattice distortions caused by doping Fe with different ionic radius has increased the oxygen vacancies in Fe doped samples [31,32]. Table 2 confirms the presence of higher amounts of vacancies in case of $Mn_{1.8}Fe_{0.2}O_3$ sample. According to the literature, the presence of higher amount of oxygen vacancies will lead to higher catalytic soot activity [33]. So it can be expected that $Mn_{1.8}Fe_{0.2}O_3$ sample might give better catalytic activity compared to other materials.

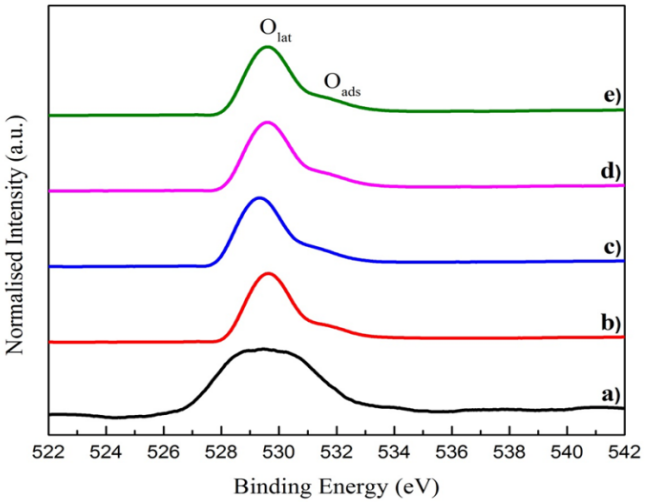

Figure 4: XPS of O1s core level spectra for all the samples, where a) Mn_2O_3, b) $Mn_{1.95}Fe_{0.05}O_3$, c) $Mn_{1.9}Fe_{0.1}O_3$, d) $Mn_{1.85}Fe_{0.15}O_3$ and e) $Mn_{1.8}Fe_{0.2}O_3$

Table 2: $O_{adsorbed}/O_{lattice}$ peaks in the XPS of O 1s region and % composition of $Mn^{+2/+3/+4}$ and $Fe^{+2/+3}$ cations.

S.No	Sample	% O species		% Mn species			% Fe species	
		O_{lat}	O_{ads}	Mn^{+2} (640eV)	Mn^{+3} (641.3 & 652.9 eV)	Mn^{+4} (642eV)	Fe^{+2} (712.4 & 716eV)	Fe^{+3} (710 & 723.9 eV)
1.	Mn_2O_3	82	18	0	73.47	26.53	0	0
2.	$Mn_{1.95}Fe_{0.05}O_3$	72	27	13.72	67.14	19.13	50	50
3.	$Mn_{1.9}Fe_{0.1}O_3$	71	29	14.76	64.62	20.62	56	44
4.	$Mn_{1.85}Fe_{0.15}O_3$	69.2	30.8	16.74	62.19	21.07	66	34
5.	$Mn_{1.8}Fe_{0.2}O_3$	67.92	32.07	18.36	60.94	19.68	39	61

FESEM Analysis

Apart from the redox behavior of the samples, the morphology also plays a vital role in the soot oxidation activity [34]. In order to understand the structure of the samples FESEM analysis was performed on all the prepared samples. The SEM images of the Fe-doped and pure Mn_2O_3 are displayed in Figure.5. As depicted from the micrograph 5(a), a spherical sponge like nanostructures was formed. There is no particular change in the morphology of the samples upon doping with Fe. However, as the Fe dopant level (x) increases the catalysts looks to be comparatively more porous and uniform as observed from the increase in pore volume in Table 1 [35]. The presence of porous structure aids in providing good contact between soot and catalyst during the soot oxidation reaction, which might improve the catalytic soot oxidation activity [36]. Among all the samples prepared, $Mn_{1.8}Fe_{0.2}O_3$ sample has a good porosity (high pore volume) which might aid in the increase in soot oxidation activity for this material

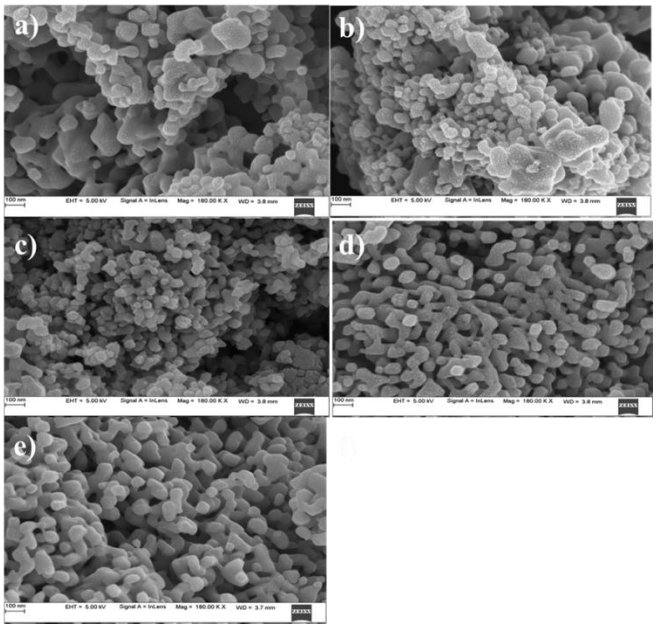

Figure 5: FESEM Images of all the prepared samples, where a) Mn_2O_3 b) $Mn_{1.95}Fe_{0.05}O_3$ c) $Mn_{1.9}Fe_{0.1}O_3$ d) $Mn_{1.85}Fe_{0.15}O_3$ and e) $Mn_{1.8}Fe_{0.2}O_3$

Catalytic Soot Oxidation Activity-TGA Analysis

From the above characterization results, it can be expected that Fe doped Mn_2O_3 samples would give better soot oxidation activity when compared to the undoped one. And among the iron doped samples $Mn_{1.8}Fe_{0.2}O_3$ might have improved soot conversion activity. To confirm with these interpretations, soot oxidation activity on the prepared samples was performed in TGA instrument in the temperature range of 200-700°C.

Figure.6. represents the % soot conversion profiles of uncatalyzed soot and catalyzed soot under tight conditions as a function of temperature. The temperature T_{50}°C i.e, the temperature at which the 50% of the soot is oxidized is summarised in Table 3. It can be seen from the figure that for bare soot the 50% of soot conversion happened at around 600°C. The soot oxidation activity increased with the addition of catalyst and is in the order of $Mn_{1.8}Fe_{0.2}O_3$> $Mn_{1.85}Fe_{0.15}O_3$> $Mn_{1.9}Fe_{0.1}O_3$> $Mn_{1.95}Fe_{0.05}O_3$> Mn_2O_3> Soot.

Shangguan et al. stated that adsorbed oxygen species show a dynamic role in the soot oxidation process [37]. Addition of Mn_2O_3 catalyst during the soot oxidation has markedly reduced the soot oxidation temperature to 490°C similar to the reported literature so far [38] unlike other oxides like Al_2O_3 [39]. The presence of redox stability (as confirmed by XPS analysis) in Mn and also the existence of adsorbed oxygen on the surface has increased the soot oxidation activity in this material. However doping of Mn_2O_3 lattice with Fe has remarkably increased the soot conversion in comparison with Mn_2O_3. Addition of Fe into Mn lattice has created more lattice distortions in the samples as noted from the XRD analysis. This doping has also increased the amount of adsorbed oxygen in these samples which might be due to the redox ability of Fe along with Mn as seen from XPS analysis. This has led to the increase in soot oxidation activity in Fe doped Mn samples. It can also be noticed that Fe doped samples appear to be more porous when compared to the undoped one (FESEM analysis). This porous nature in these samples has increased the contact between the soot and catalyst which is also a reason behind high catalytic activity in $Mn_{2-x}FexO_3$ samples. The soot oxidation results show that among all the samples prepared, $Mn_{1.8}Fe_{0.2}O_3$ have higher soot conversion. This is due to the fact that, this sample has high surface area, more porous structure and also higher amount of surface adsorbed oxygen when compared to all other Fe doped samples.

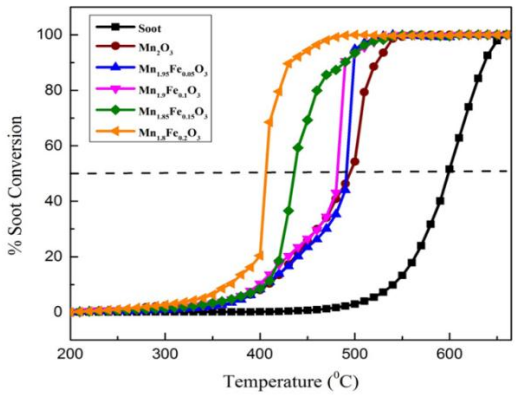

Figure 6: Profile for Soot Oxidation Activity of all the samples

Based on the literature reported [40] we propose a mechanism as follows. This soot oxidation process involves the active oxygen species through adsorption of oxygen on the reduced metal surface (Mn^{+3}/Fe^{+2}) and subsequent electron transfer metal cations at the interface between soot and catalyst ($Mn_{2-x}Fe_xO_3$). Among the four different level of Fe doping, $Mn_{1.8}Fe_{0.2}O_3$ oxidized soot at a lower temperature of 400°C comparatively. The reason for this might be due to the formation of a huge number of defects in the Mn_2O_3 cubic crystal lattice because of a higher level of Fe doping and subsequent generation of active adsorbed oxygen species in abundant amounts which are responsible for high soot oxidation activity.

$$M^n - O_v + O_{2(gas)} \rightarrow M^{n+1} - O_{ads}$$

$$or$$

$$O_{2(gas)} \Leftrightarrow [O_{ads}]$$

$$S_f + O_{ads} \rightarrow SOC$$

$$SOC + O_{ads} / O_{2(gas)} \rightarrow CO / CO_2$$

Where, M-metal cations, O_{ads} is the adsorbed oxygen species, S_f is a free site on soot and SOC is the Soot Oxygen Complex which is an intermediate reacts with either $O_{2(gas)}$ or O_{ads} to form soot oxidation products. On summarizing, the incorporation of Fe^{+3}/Fe^{+2} ions into the Mn_2O_3 lattice improved the redox property of Mn (+2/+3/+4) thereby enhancing the formation of efficient adsorbed oxygen species.

CONCLUSION

Cost effective Fe-doped Mn_2O_3 basically $Mn_{2-x}Fe_xO_3$ (x=0.05 to 0.2) catalysts were effectively synthesized by co precipitation method for the application of soot oxidation and characterized by various analysis such as XRD, BET, XPS and FESEM, The capability of thus synthesized catalysts in reducing the soot oxidation temperatures was evaluated with the help of TG-DTA analysis. The redox stability in Mn and presence of surface adsorbed oxygen in the Mn_2O_3 crystal played an important role in improving the catalytic oxidation of soot. Addition of Fe to Mn_2O_3 has increased the amount of adsorbed oxygen, caused due to the structural distortions upon doping and also due to the redox stability of Fe which thereby increased the soot conversion activity in $Mn_{2-x}Fe_xO_3$ samples. Amongst the Fe substituted compounds $Mn_{1.8}Fe_{0.2}O_3$ exhibited the highest activity. The ability of this particular catalyst can be attributed to the improved redox property and also the formation of huge amounts of stable adsorbed oxygen species in this sample.

Table 3: $T_{1/2}$ temperatures for the soot oxidation

S.No	Sample	$T_{1/2}$ (°C)
1.	Mn_2O_3	490
2.	$Mn_{1.95}Fe_{0.05}O_3$	470
3.	$Mn_{1.9}Fe_{0.1}O_3$	455
4.	$Mn_{1.85}Fe_{0.15}O_3$	420
5.	$Mn_{1.8}Fe_{0.2}O_3$	400

REFERENCES

[1] F. Laden, J. Schwartz, F. E. Speizer, and D. W. Dockery, "Reduction in Fine Particulate Air Pollution and Mortality Extended Follow-up of the Harvard Six Cities Study," no. 7, 1998.

[2] T. Wang, S. Li, Y. Shen, J. Deng, and M. Xie, "Investigations on direct and indirect effect of nitrate on temperature and precipitation in China using a regional climate chemistry modeling system," vol. 115, pp. 1–13, 2010.

[3] F. Laden and D. Dockery, "Chronic Exposure to Fine Particles and Mortality : An Extended Follow-up of the Harvard Six Cities Study from 1974 to 2009" pp. 3–9, 2017.

[4] A. M. K. Naapen, P. J. A. B. Orm, C. A. Lbrecht, and R. P. F. S. Chins, "Mini Review Inhaled Particles And Lung Cancer . Part A : Mechanisms Int. J.Cancer,109,799-809,2004.

[5] O. Deutschmann and A. G. Konstandopoulos, Catalytic Technology for Soot and Gaseous Pollution Control, vol. 2, no. x. 2010.

[6] A. Setiabudi, M. Makkee, and J. A. Moulijn, "The role of NO_2 and O_2 in the accelerated combustion of soot in diesel exhaust gases," vol. 50, no. 2, pp. 185–194, 2004.

[7] N. Guilhaume, B. Bassou, G. Bergeret, D. Bianchi, F. Bosselet, B. Jouguet, C. Mirodatos, "In situ investigation of Diesel soot combustion over an AgMnO x catalyst," *"Applied Catal. B, Environ.*, vol. 119–120, pp. 287–296, 2012.

[8] B. Bassou, N. Guilhaume, K. Lombaert, C. Mirodatos, and D. Bianchi, "Experimental Microkinetic Approach of the Catalytic Oxidation of Diesel Soot by Ceria Using Temperature-Programmed Experiments . Part 1 : Impact and Evolution of the Ceria / Soot Contacts during Soot Oxidation," no. 6, pp. 4766–4780, 2010.

[9] S. Wagloehner, J. N. Baer, and S. Kureti, "Structure – activity relation of iron oxide catalysts in soot oxidation," *Applied Catal. B, Environ.*, vol. 147, pp. 1000–1008, 2014.

[10] S. Waglöhner, D. Reichert, H. Bockhorn, and S. Kureti, "Studies on the Effect of Physico-Chemical Soot Properties and Feed Gas Composition on the Kinetics of Soot Oxidation on Fe_2O_3 Catalyst," no. 5, pp. 686–695, 2013.

[11] Z. Zhang, D. Han, S. Wei, and Y. Zhang, "Determination of active site densities and mechanisms for soot combustion with O_2 on Fe-doped CeO 2 mixed oxides," *J. Catal.*, vol. 276, no. 1, pp. 16–23, 2010.

[12] R. K. K. A. V Salker, "Activity of Pd doped and supported Mn 2 O 3 nanomaterials for CO oxidation," pp. 395–405, 2012.

[13] P. Kar, S. Sardar, S. Ghosh, M. Parida, B. Liu, O. F. Mohammed, P. Lemmens and S. K. Pal, "Nano Surface Engineering of Mn_2O_3 for Potential Light-Harvesting Application" J. Mater. Chem.2015

[14] D. Mukherjee, B.G. Rao, B.M. Reddy, CO and Soot Oxidation Activity of Doped Ceria: Influence of Dopants. Appl. Catal. B Environ., 197, 105–115, 2016.

[15] D. Mishra, R. Arora, S. Lahiri, S. S. Amritphale, and N. Chandra, "Synthesis and Characterization of Iron Oxide Nanoparticles by Solvothermal Method" vol. 50, no. 5, pp. 628–631, 2014.

[16] F. Lin, R. Delmelle, T. Vinodkumar, B. M. Reddy, A. Wokaun, and I. Alxneit, "Correlation between the structural characteristics, oxygen storage capacities and catalytic activities of dual-phase Zn-modified ceria nanocrystals," *Catal. Sci. Technol.*, vol. 5, no. 7, pp. 3556–3567, 2015.

[17] W. Y. Hernandez, M. N. Tsampas, C. Zhao, A. Boreave, F. Bosselet, and P. Vernoux, "La/Sr-based perovskites as soot oxidation catalysts for Gasoline Particulate Filters," *Catal. Today*, vol. 258, pp. 525–534, 2015.

[18] F. Li, L. Zhang, D. G. Evans, and X. Duan, "Structure and surface chemistry of manganese-doped copper-based mixed metal oxides derived from layered double hydroxides," vol. 244, pp. 169–177, 2004.

[19] E. Aneggi, V. Cabbai, A. Trovarelli, and D. Goi, "Potential of Ceria-Based Catalysts for the Oxidation of Landfill Leachate by Heterogeneous Fenton Process," doi:10.1155/2012/694721, 2012.

[20] W. R. Knocke, A. M. Dietrich, and T. F. Cromer, "Use of XPS to Identify the Oxidation State of Mn in Solid Surfaces of Filtration Media Oxide Samples from Drinking Water Treatment Plants," vol. 44, no. 15, pp. 5881–5886, 2010.

[21] M. A. Stranick, "Mn_2O_3 by XPS," vol. 6, no. 1, pp. 39–46, 1999.

[22] D. B. Anerjee, "Interpretation of XPS Mn (2p) spectra of Mn oxyhydroxides and constraints on the mechanism of MnO_2 precipitation," vol. 83, no. 1994, pp. 305–315, 1998.

[23] X. Wu, S. Liu, D. Weng, F. Lin, and R. Ran, "MnO_x–CeO_2–Al_2O_3 mixed oxides for soot oxidation : Activity and thermal stability," vol. 187, pp. 283–290, 2011.

[24] A.S. Science, S. Elettrontca, C. Spettrochrmico, V. Salaria, M. Scala, F.P. Model, N. Fe, V.G. Esca "Xps

analysis e. paparazzo of iron aluminum oxide systems," 1986.

[25] T. Yamashita and P. Hayes, "Analysis of XPS spectra of Fe^{2+} and Fe^{3+} ions in oxide materials," vol. 254, pp. 2441–2449, 2008.

[26] Æ. L. M. Æ, N. D. Abazovic, and I. A. Jankovic, "Synthesis and Characterization of Rutile TiO_2 Nanopowders Doped with Iron Ions," pp. 518–525, 2009.

[27] M. Buchalska, M. Kobielusz, A. Matuszek, M. Pacia, S. Wojty, and W. Macyk, "On oxygen activation at rutile- and anatase-TiO_2," 2015.

[28] C. Chang and T. Huanp, "A Solid-state Electrochemical Study of Adsorbed Oxygen Species in the Light-Off Phenomenon of CO Oxidation over Platinum Catalysts," pp. 2364–2370, 1995.

[29] D. A. Pawlak, M. Ito, M. Oku, K. Shimamura, and T. Fukuda, "Interpretation of XPS O (1s) in mixed oxides proved on mixed perovskite crystals," J. Phys. Chem. B, vol. 106, no. 2, pp. 504–507, 2002.

[30] W. Yao, Æ. R. Wang, and Æ. X. Yang, "$LaCo_{1-x}Pd_x O_3$ Perovskite-Type Oxides : Synthesis , Characterization and Simultaneous Removal of NO_x and Diesel Soot," no. x, pp. 613–621, 2009.

[31] A. Yokozawa, A. Oshiyama, Y. Miyamoto, and S. Kumashiro, "Oxygen Vacancy with Large Lattice Distortion as an Origin of Leakage Currents in SiO," pp. 703–706, 1997.

[32] M. Lorenz, B. Rolf, S. Friedl, P. Andreas, D. Spemann, and M. Grundmann, "Local lattice distortions in oxygen deficient Mn- doped ZnO thin films , probed by electron paramagnetic resonance," pp. 4947–4956, 2014.

[33] Z. Zhong, K. Chen, Y. Ji, and Q. Yan, "prepared by sol-gel method," vol. 156, 1997.

[34] P. Miceli, S. Bensaid, N. Russo, and D. Fino, "Effect of the morphological and surface properties of CeO_2-based catalysts on the soot oxidation activity," *Chem. Eng. J.*, vol. 278, pp. 190–198, 2015.

[35] Han Zhao, Xiaoxia Zhou, Min Wang, Zhiguo Xie, Hangrong Chen, Jianlin Shi, "Highly active MnO_x-CeO_2 catalyst for soot combustion," RSC Adv., 7, pp. 3233–3239, 2017.

[36] W. Shao, Z. Wang, X. Zhang, and L. Wang, "Promotion Effects of Cesium on Perovskite Oxides for Catalytic Soot Combustion," *Catal. Letters*, vol. 146, no. 8, pp. 1397–1407, 2016.

[37] W. F. Shangguan, Y. Teraoka, and S. Kagawa, "Kinetics of Soot-O Soot-NO and Soot-O-NO Reactions over Spinel-Type CuFeO Catalyst," Appl. Catal. B Environ.,vol. 12, pp. 237–247, 1997.

[38] A. P. Anantharaman, H. Prasad, D. Jong, H. Lee, and H. Dasari, "Soot Oxidation Activity of Redox and Non-Redox Metal Oxides Synthesised by EDTA – Citrate Method," *Catal. Letters*, vol. 0, no. 0, p. 0, 2017.

[39] D. Harshini, C. W. Yoon, J. Han, S. P. Yoon, S. W. Nam, and T.-H. Lim, "Catalytic Steam Reforming of Propane over Ni/LaAlO3 Catalysts: Influence of Preparation Methods and OSC on Activity and Stability," *Catal. Letters*, vol. 142, no. 2, pp. 205–212, 2012.

[40] B. R. Stanmore, J. F. Brilhac, and P. Gilot, "The oxidation of soot : a review of experiments , mechanisms and models," vol. 39, pp. 2247–2268, 2001.